Characteristics of SME Biodiesel-Fueled Diesel Particle Emissions and the Kinetics of Oxidation

HEEJUNG JUNG,[†]
DAVID B. KITTELSON,*,[‡] AND
MICHAEL R. ZACHARIAH[§]

Department of Mechanical and Aeronautical Engineering and Land, Air and Water Resources, University of California— Davis, One Shields Avenue, Davis, California 95616, Department of Mechanical Engineering, University of Minnesota, 111 Church Street, S.E., Minneapolis, Minnesota 55455, and Department of Chemistry and Biochemistry and Department of Mechanical Engineering, University of Maryland, College Park, Maryland 20742

Biodiesel is one of the most promising alternative diesel fuels. As diesel emission regulations have become more stringent, the diesel particulate filter (DPF) has become an essential part of the aftertreatment system. Knowledge of kinetics of exhaust particle oxidation for alternative diesel fuels is useful in estimating the change in regeneration behavior of a DPF with such fuels. This study examines the characteristics of diesel particulate emissions as well as kinetics of particle oxidation using a 1996 John Deere T04045TF250 off-highway engine and 100% soy methyl ester (SME) biodiesel (B100) as fuel. Compared to standard D2 fuel, this B100 reduced particle size, number, and volume in the accumulation mode where most of the particle mass is found. At 75% load, number decreased by 38%, DGN decreased from 80 to 62 nm, and volume decreased by 82%. Part of this decrease is likely associated with the fact that the particles were more easily oxidized. Arrhenius parameters for the biodiesel fuel showed a 2−3 times greater frequency factor and ∼6 times higher oxidation rate compared to regular diesel fuel in the range of 700−825 °C. The faster oxidation kinetics should facilitate regeneration when used with a DPF.

Introduction

Knowledge of the kinetics of diesel particle oxidation is indispensable in the design of low-emission engines and aftertreatment systems. Although there have been many kinetic studies of oxidation of soot emitted by flames and by diesel engines operating on petroleum-based fuels, little information is available on the oxidation of particles formed by biodiesel fuels. Song et al. (*1, 2*) compared oxidation of biodiesel soot with other diesel soot by thermo-gravimetric analysis (TGA). However, the TGA method has been criticized by Mahadevan et al. (*3*) and others because of uncertainties associated with separating heat and mass transfer effects

from the underlying chemical kinetics. The current study used the high-temperature oxidation-tandem differential mobility analysis (HTO-TDMA) technique which avoids heat and mass transfer limitations and has not been used before with biodiesel fuel. It is discussed in detail later. Possible indirect evidence of increased oxidation rates with biodiesel is found in recent work by Mayer et al. (*4*). They investigated the impact of rapeseed (RME) based biodiesel blends on emissions and trap performance using a continuously regenerating trap type DPF. They did not report significant changes in DPF regeneration behavior despite significantly lower exhaust temperatures. This could be due to faster oxidation kinetics with the RME blend.

In this study the kinetics of particle oxidation, as well as particle concentrations and size, have been measured for particles emitted by a diesel engine operating on a 100% soy methyl ester (SME) biodiesel fuel (B100). HTO-TDMA was employed to measure surface-specific oxidation rates from size-selected diesel exhaust particles over the temperature range of 700−825 °C. The change in particle diameter after oxidation took place was measured and converted into the surface-specific oxidation rate. Particle size distributions were measured using a scanning mobility particle sizer (SMPS) (*5*). The contribution of volatile materials to the size distribution was examined using a catalytic stripper along with the SMPS.

Background Information on Biodiesel

Biodiesel is a generic term that refers to various fatty-acid mono-esters that can be used for diesel fuel. It is made from the conversion of triglyceride (vegetable oil and animal fats) to esters (primarily methyl esters) via various esterification processes (*6*). Biodiesel has physical properties very similar to those of conventional diesel fuel (*7*); but it is renewable, nontoxic, and biodegradable (*8*). Biodiesel is the only alternative fuel to have fully completed the health effects testing requirements of the Clean Air Act. It may be made from a variety of different vegetable oils or animal fats. For example, in Germany rapeseed-oil-based biodiesel, RME, is the most abundant (*9*), whereas soy-based biodiesel, SME, the fuel used in this study, is the most widely used in the United States (*10*).

Biodiesel can be blended in any proportion with petroleum diesel fuel, and blended biodiesel, mainly in blends of 20% (B20) or less, can be used in most conventional diesel engines with little or no modification. However, only a few manufacturers recommend operating their engines with blends higher than B5. However, it is likely that this value of blend ratio will increase as biodiesel fuel quality improves and appropriate additives are developed.

There are advantages and disadvantages to using biodiesel as compared to using petroleum-based diesel fuel. Advantages include biodiesel's greater cetane number than D2 (regular diesel fuel) (*11*), and the fact that biodiesel contains essentially no aromatics or sulfur. The absence of sulfur reduces corrosion and prevents sulfur poisoning of aftertreatment systems. Biodiesel is oxygenated fuel with high oxygen content, ∼11% (*7, 11*), which reduces elemental carbon emissions. There are also disadvantages to biodiesel fuel. It has slightly lower fuel density than regular diesel fuel, so more fuel is required to achieve the same amount of power. Compared to regular diesel fuel, biodiesel also has higher viscosity, affecting spray formation; higher pour point and cloud points, limiting winter operation; lower oxidative stability, shortening storage life; and higher organic carbon emissions.

* Corresponding author phone: 612-625-1808; fax: 612-624-1578; e-mail: kitte001@umn.edu.
[†] University of California—Davis.
[‡] University of Minnesota.
[§] University of Maryland.

TABLE 1. Fuel Analysis of Regular Petroleum Based Diesel Fuel (D2) and 100% Soy Methyl Esters (SME) Biodiesel (B100)

property	unit	ASTM	D2	SME B100
flash pt.	°C	D93	71	160
heating value	BTU/lb	D240	18111	15873
kinematic viscosity	cSt @ 40 °C	D445	2.74	4.891
cetane number		D613	44.9	50
specific gravity	g/mL @ 15 °C	D1298	0.848	0.883
aromatics	vol. %	D1319	27.6	
sulfur	mass %	D2622	0.031	0
cloud pt.	°C	D5773	−29	0
free and total glycerin		D6584		
free glycerin	mass %			0.006
monoglyceride	mass %			0.59
diglyceride	mass %			0.283
triglyceride	mass %			0.009
glycerin	mass %			0.202

Emissions of total PM, CO, and HC are reduced by using biodiesel fuel (*10, 12*), while those of particle-bound volatile organic material (organic carbon) are increased (*13, 14*), and those of NO$_x$ are slightly higher (*10, 12*) However, recent work suggests that NO$_x$ emissions either increase or decrease slightly depending upon the vehicle and test condition (*15*). Oxidation catalysts allow for effective control of organic carbon (*11, 16*). Various approaches to reduce NO$_x$ have been proposed, such as fuel additives (*17*), using water emulsions with exhaust gas recirculation (EGR) (*18*), using sensors to detect the presence of biodiesel and shift injection timing accordingly (*19*), and modifying soybean oil composition to enhance methyl oleate content (*20, 21*). Other environmental effects resulting from the use of biodiesel as fuel include a slight increase of ozone precursors (*12*), but a reduction in elemental carbon, a global warming agent.

In general it is reported that biodiesel has a less adverse effect on human health than petroleum-based diesel fuel. Schröder et al. (*9*) and Krahl et al. (*12*) reported that mutagenicity of biodiesel particulate emissions is much lower than that of petroleum-based fuel. Finch et al. (*22*), in their study of rats exposed to biodiesel emissions, showed only modest health effects at the highest exposure level. Even these effects were described as "no-observed-adverse-effect" within the uncertainties of their study.

Europe is the most significant biodiesel producer in the world (*23, 24*). Germany and France lead the production and give a tax benefit for producing biodiesel. Brazil launched a national program for biodiesel in 2002 (*25*) and leads the production in South America, producing biodiesel for both domestic use and export (*26*).

Experimental Section

Fuel Properties and Lubricating Oil. A standard EPA No. 2 on-road diesel fuel and 100% soy methyl ester (SME) biodiesel were used in this study. Both the biodiesel and the D2 were purchased from a commercial supplier (Yocum Oil Company Inc., St. Paul, MN). Although it is unusual to use more than 20% biodiesel (B20), in this study 100% biodiesel (B100) was used to allow the kinetics of oxidation to be clearly defined.

Table 1 shows fuel properties obtained using ASTM standard methods. The biodiesel has a higher cetane number, cloud point, and flash point than D2. The properties are similar to those reported by Bagley et al. (*11*) and Monyem and van Gerpen (*27*). The lubricating oil used in this study was SAE15W-40 (John Deere TY6391). The detailed lubricating oil properties can be found in a previous study (*28*).

Engine, Sampling, and Dilution System. The engine used in this study was a 1996 John Deere T04045TF250, which is a medium-duty, off-highway, direct-injection, 4 cylinder, 4 cycle, turbocharged diesel engine. It had a 4.5 L displacement, with a peak power output of 125 HP (93 kW) at 2400 rpm and
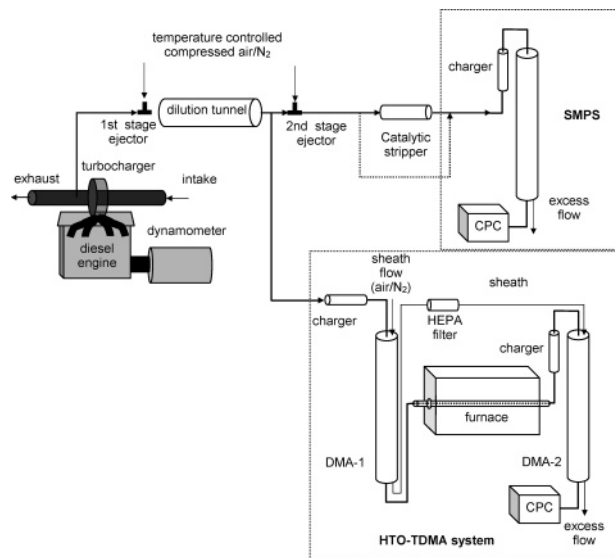
FIGURE 1. Schematic diagram of experimental setup. The bold line indicates the path taken by the diesel particles.

a peak torque output of 400 N·m at 1400 rpm. The engine was loaded with a dynamometer for load control. It was operated at 1400 rpm under 75% load (300 N·m) for the oxidation study, and at 10, 50, and 75% load for size distribution measurements.

Figure 1 shows a schematic diagram for the engine bench, sampling system, scanning mobility particle sizer (SMPS), and high-temperature oxidation-tandem differential mobility analyzer (HTO-TDMA) system (*29*). The exhaust was sampled 25 cm downstream of the turbocharger exit, and was diluted in a two stage, ejector type, variable residence time dilution tunnel, similar to the one described by Abdul-Khalek and Kittelson (*30*). For the oxidation study, particles were extracted after the first stage of dilution, which was operated with a fixed residence time of 0.8 s at a dilution ratio of 26−28:1 for 75% load at 1400 rpm.

The first stage dilution ratio was determined by comparing the NO$_x$ concentration in the exhaust gas and in the diluted exhaust gas; corrections were made for the background NO$_x$ concentration. The first stage dilution air temperature was maintained at 32 °C by preheating and temperature stabilizing the compressed air to the ejector.

All size distribution samples were taken after the second stage of dilution to prevent saturation of the condensation particle counter (CPC) (model 3025A, TSI Inc.). The second stage dilution ratio was determined by flow measurements to be 31:1. Thus, the overall dilution ratio after the second stage was 810−870:1, calculated using the product of the dilution ratios for each stage.
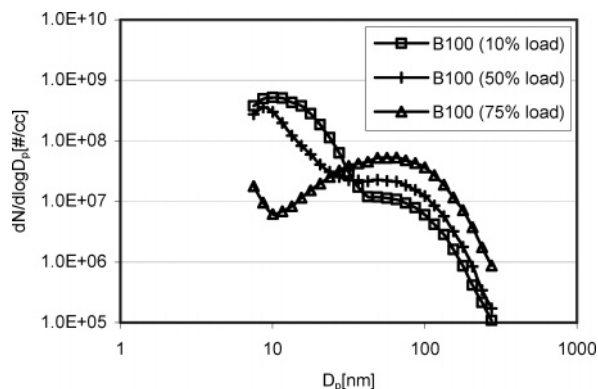
FIGURE 2. Size distributions of diesel particles with biodiesel (B100) fuel for various engine loads at 1400 rpm.

Scanning Mobility Particle Sizer (SMPS). The SMPS system was used for size distribution analysis. The SMPS measures mobility equivalent particle diameter in the diameter range of 7−300 nm during a 4-minute (2 min up, 2 min down) scan time. This particle measurement system consists of a neutralizer, a mobility section (long column DMA similar to TSI model 3934) with a sampling flow rate of 1 Lpm and a sheath flow rate of 10 Lpm, a CPC (TSI model 3010), and a computerized control and data acquisition system. This system has been described in more detail by others (*30, 31*).

Catalytic Stripper. The catalytic stripper (CS) is a small catalytic converter that is maintained at a constant temperature (300 °C) to evaporate and subsequently oxidize volatile organic materials in the exhaust particulate matter (*32*). Volatile organics diffuse to the catalyst-coated wall of the stripper and oxidize on the catalyst-coated wall. Volatile sulfur compounds are also removed by capture in the catalyst wash coat. Size distribution data, with and without the catalytic stripper, give information on how much particle phase volatile material is present, especially in the nuclei mode size range, i.e., diameter less than about 30 nm (*28, 33−35*).

High-Temperature Oxidation-Tandem Differential Mobility Analyzer (HTO-TDMA). Particle oxidation rates were determined using the HTO-TDMA as described in detail by Higgins et al. (*29*). Briefly, in the HTO-TDMA, the sample is sent through a bipolar diffusion charger to establish a known charge distribution. Next, a specific particle size is selected with DMA-1. The DMA selects mono-area particles based on electrical mobility. These particles are then oxidized in air by passing them through a quartz flow tube enclosed in a tube furnace of known residence time and temperature profile. The particles are recharged in a bipolar diffusion charger, and the size change resulting from the high-temperature processing (which includes oxidation, thermal restructuring, and evaporation) is measured by scanning DMA-2. Three initial particle sizes of 40, 89, and 128 nm mobility diameters were selected at DMA-1 to match the previous study on diesel nanoparticle oxidation (*29*). Furnace temperature settings ranged from room temperature (25−34 °C, depending on the day) to 825 °C.

To check for particle size changes due to thermal restructuring effects, additional experiments were conducted by using nitrogen as a carrier gas in both the first stage dilution and DMA sheath flows in our previous study (*29*).

Results and Discussion

Figure 2 shows exhaust particle size distributions (corrected for dilution ratio) as a function of engine load at 1400 rpm using biodiesel as fuel. Trends seen for biodiesel fuel were similar to those measured earlier with this engine using
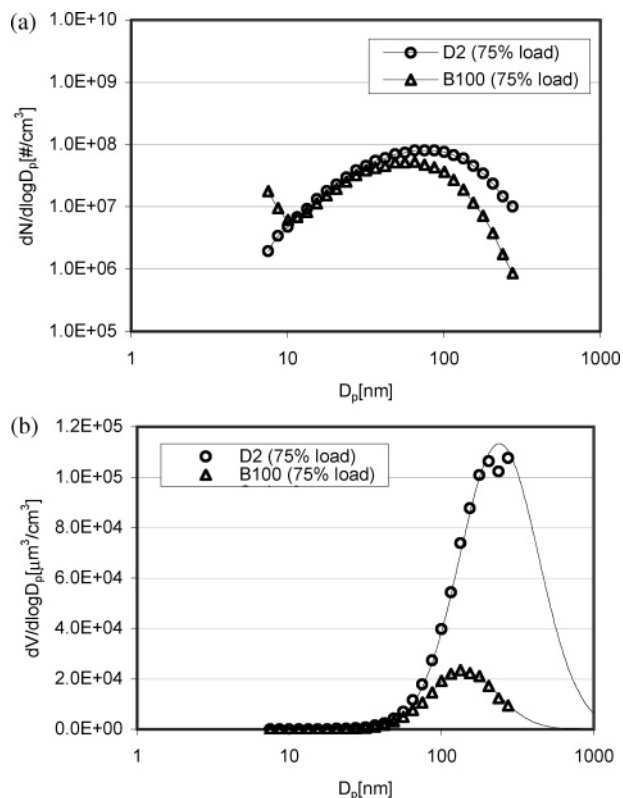
FIGURE 3. Size distributions of diesel particles with biodiesel (B100) fuel and petroleum based regular diesel fuel (D2) at 1400 rpm, 75% load: (a) number distributions, and (b) volume distributions.

regular petroleum-based fuel (D2) (*35*). For both types of fuel, the accumulation mode increased and the nuclei mode decreased as engine load increased. However, the nucleation mode for biodiesel was relatively larger and the accumulation mode was smaller than that observed earlier with D2. The reduction in the accumulation mode compared to D2 is apparent in Figure 3a and b, which compares size distributions measured at 1400 rpm, 75% load using biodiesel and D2. As seen in Figure 3, the concentrations of particles larger than about 50 nm are markedly reduced using biodiesel, leading to a decrease in the geometric number mean diameter of the accumulation mode (DGN) from 80 to 62 nm and reductions of accumulation mode number and volume concentrations of 38% and 82%, respectively. The accumulation mode is where most of the particle volume, mass, and elemental carbon are usually found (*36*). Thus, the reduction in accumulation mode volume is consistent with other studies (*11, 12*) showing reductions of diesel particulate mass (DPM) with biodiesel. The reduction of accumulation mode volume concentration may be due to a combination of factors. Combustion timing is more advanced with biodiesel due to its higher cetane number and physical properties (*10*). Monyem and van Gerpen (*10*) showed that more advanced combustion timing reduces soot and increases NO_x for both B100 and D2. Further, biodiesel contains about 11% oxygen, and there have been many studies showing that the presence of oxygen in fuel reduces soot formation (*37, 38*). Another factor may be the greater reactivity of these particles demonstrated by the oxidation kinetics measurements described below.

The catalytic stripper (CS) was placed ahead of the SMPS to examine how much volatile material was present in diesel particles using biodiesel as fuel. Sakurai et al. (*39*) have shown that when diesel particles are heated to temperatures as high as 300−400 °C, they may be classified into two types, ''less volatile'' ones that shrink only slightly, and ''more volatile''

(a) 1.0E+08

dN/dlogD_p[#/cc]

- △ without stripper
- ■ with stripper
- × with stripper after loss correction

D_p[nm]

(b) 6.0E+07

dN/dlogD_p[#/cc]

- △ without stripper
- × with stripper after loss correction
- ◇ Volatiles dist.

D_p[nm]
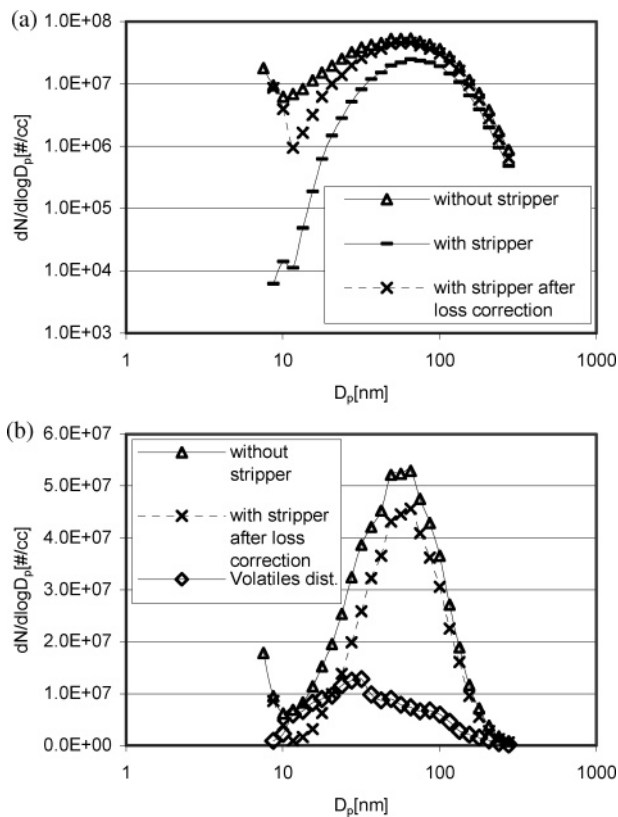
FIGURE 4. Size distributions of diesel particles with and without a catalytic stripper at 1400 rpm, 75% load using B100 fuel. Dotted line with "x" mark shows size distribution with a catalytic stripper after transport (diffusion and thermophoresis) loss correction: (a) y-axis in log scale, and (b) y-axis in linear scale for volatile species distribution.

FIGURE 5. TDMA diesel particle oxidation results in air for furnace settings of 30—800 °C: 89 nm initial particle size with B100 biodiesel.

ones that almost completely disappear. The "more volatile" ones were identified to be mainly heavy hydrocarbons and some sulfate, the "less volatile" ones were identified as carbonaceous agglomerates, although most of the volatile materials associated with PM are usually found adsorbed on these agglomerates. The reason that agglomerates do not shrink significantly upon heating is that their external envelope (which determines their drag and thus their mobility size) is not strongly influenced by desorption of volatiles.

Size distributions with and without the CS are compared in Figure 4a and b for the 1400 rpm, 75% load condition. The material remaining after correcting for transport losses (thermophoretic and diffusion) in the catalytic stripper is material that is nonvolatile at 300 °C, mainly elemental carbon and lubricating oil ash. Most of the material in the accumulation mode above about 100 nm is nonvolatile, presumably mainly elemental carbon. There is evidence of a secondary nonvolatile mode below about 10 nm which is believed to be associated with lubricating oil ash (28, 40). The difference between the non-CS and the corrected CS size distributions is an indication of the amount of volatile material present at each size. The two size distributions shown differ the most in the 10—100 nm range, as shown in Figure 4b, which has a linear y scale, suggesting that most of the volatile particles are in this size range. It is widely known that diesel particles using biodiesel as fuel contain more volatile matter (13, 14). Our study shows the amount of volatile matter is a function of particle size.

Figure 5 shows representative HTO-TDMA data for 89 nm particles generated using biodiesel at 1400 rpm, 75% load. Results for the other initial particle sizes tested (40 and 128 nm) are not presented here but are similar. Figure 5
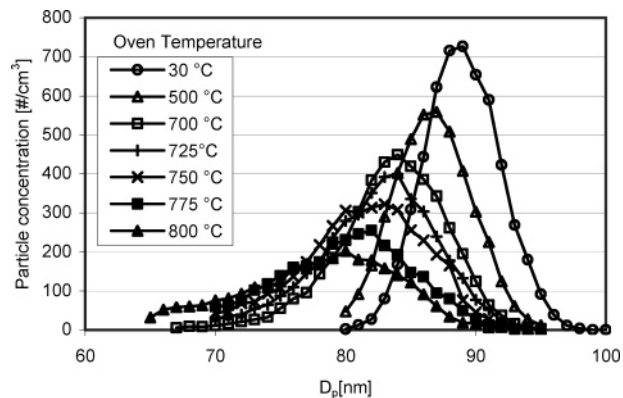
illustrates that the particles shrink as the furnace temperature increases, and that the mobility diameter decreases by 2 nm at 500 °C and 9 nm at 800 °C. The initial shrinkage in size below 500 °C is likely due to desorption or evaporation of volatile materials. Higgins et al. (29) found that the total particle size decrease, due to non-oxidative effects at 500 °C, measured using nitrogen as the carrier gas, amounted to ~1 nm at 75% load using regular diesel fuel. The larger 2 nm shrinkage we observed at 500 °C using biodiesel can be attributed to the presence of more volatile PM with biodiesel. Above 500 °C, most of the change in diameter is a result of particle oxidation. In addition to a decrease in particle size with increasing oven temperature, we also observed a decrease in the number of particles. This decrease is not associated with chemical reactivity; rather, it is associated with thermophoretic transport losses, which become more important at higher temperatures (41).

Using the measured decrease in particle size, we obtained kinetic parameters following the procedure detailed in our previous studies (29, 41). The size decrease rate was modeled using a modified Arrhenius expression

$$\dot{D}_p = -A_{nm} \cdot T^{1/2} \cdot \exp\left[-\frac{E_a}{RT}\right] \quad (1)$$

where A_{nm} is an initial-size-dependent preexponential factor and E_a is a size-independent activation energy. The size decrease was determined relative to that at 500 °C for the reasons described above. Values of the A_{nm}s and E_a were determined by integrating

$$\Delta D_p = \int_0^X \frac{\dot{D}_p(x)}{u(x)} \, dx \quad (2)$$

where x is the horizontal position in the tube, X is the length of the tube, and u is the flow velocity over the heated length of the flow tube. Minimizing the differences between calculated and measured ΔD_ps was done using a nonlinear least-squares method. The dependence of the size decrease rate and flow velocity on a horizontal position is a result of their dependence on temperature as seen in eqs 1 and 3

$$u(x) = \frac{4}{3} u_m \frac{T(x)}{T_o} \quad (3)$$

where u_m is the mean flow velocity calculated from the volume flow rate and the cross-sectional area of the flow tube, and $^4/_3 u_m$ is the peak volumetric flow velocity assuming laminar flow.

Figure 6a shows experimentally determined size reductions at various oxidation temperatures for 40, 89, and 128 nm. For comparison purposes, Figure 6b shows results from
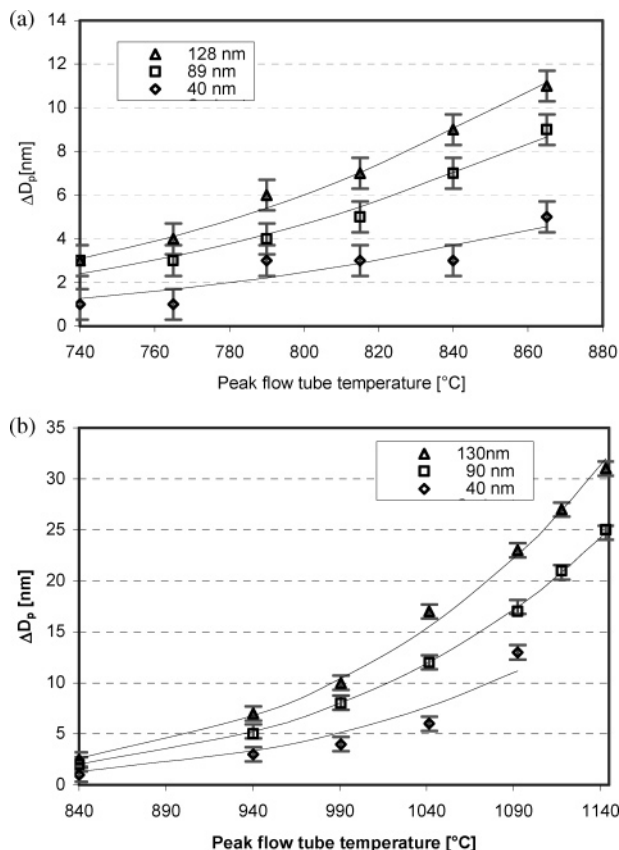
FIGURE 6. Particle size change as a function of peak flow tube temperature for the three initial particle sizes: (a) B100 biodiesel, and (b) D2 fuel (*29*).

	biodiesel
E_a [kJ mol^{-1}]	88.5
A_{40} [10^4 nm K$^{-1/2}$s^{-1}]	0.77
A_{89} [10^4 nm K$^{-1/2}$s^{-1}]	1.5
A_{128} [10^4 nm K$^{-1/2}$s^{-1}]	1.9

FIGURE 7. Arrhenius plot of the surface specific rates of diesel particle oxidation for the current study and for other relevant prior studies. Previous studies include oxidation rates of various soots (diffusion flame soot and carbon black) and pyrographite rod. HTO-TDMA studies are indicated by heavy lines. Note: Uncertainty analysis was not performed for activation energies determined by HTO-TDMA technique due to difficulties associated with the highly nonlinear nature of the fitting process. Furthermore, the fitted curves matched the data very well for most of the HTO-TDMA studies (*28, 29, 35, 41*). (a) Current study (B100 biodiesel) (89 kJ mol^{-1}); (b) Higgins et al. (*29*), diesel particles with regular diesel fuel (108 kJ mol^{-1}); (c) Jung et al. (*28*), lube oil dosed case (101 kJ mol^{-1}); (d) Jung et al. (*35*), 25 ppm cerium dosed case (107 kJ mol^{-1}); (e) Higgins et al. (*41*) using diffusion flame generated soot (164 kJ mol^{-1}); (f) Nagle and Strickland-Constable (*48*) using a pyrographite rod (143 kJ mol^{-1}); (g) Miyamoto et al. (*49*) TGA of uncatalyzed diesel soot (191 kJ mol^{-1}); (h) Gilot et al. (*50*) thermogravimetric analysis (TGA) of carbon black (103 kJ mol^{-1}); (i) Neeft et al. (*51*) flow reactor study of Printex-U flame soot from Degussa AG ($\sim$170 kJ mol^{-1}); (j) Otto et al. (*52*) TGA of diesel particles (142 $\pm$ 21 kJ mol^{-1}); (k) Ahlström and Odenbrand (*52*) flow reactor study of diesel particles (106 $\pm$ 7 kJ mol^{-1}).

our prior oxidation work using regular diesel fuel (*29*). In both cases, we observed an increase in the apparent oxidation rate with increasing initial particle size. That result was investigated in our previous study (*29*). It is necessary to correct the rates for the effective density of soot, which was measured by Park et al. (*42*) using an aerosol particle mass analyzer. Park et al. (*42*) observed that the effective density increases as the particle size decreases. Normalization to the effective density using their data resulted in an oxidation rate that was essentially particle size independent (*29*).

For practical convenience, we define the light-off temperature of oxidation as the peak-flow tube temperature, where the particle shrinks $\sim$1 nm (beyond that due to thermal evaporation). This is not the same as the light-off or balance point temperatures used in describing DPF performance which are generally much lower than those observed here. The difference is due to the much shorter reaction times, about 1 s, used in our experiments compared to DPF regeneration times. Our light-off temperatures are a fundamental measurement of particle reactivity in a system not constrained by heat and mass transfer effects. The light-off temperature was determined to be $\sim$840 °C for the regular diesel (D2) particles as shown in Figure 6b, but decreased significantly to 740 °C for biodiesel, as shown in Figure 6a. The data in Figure 6a were fitted to an Arrhenius expression (eq 1) and are shown as the solid lines on the plot. Table 2 lists the Arrhenius parameters (frequency factors, A_{nm}s, and activation energy, E_a) obtained, and Figure 7 shows Arrhenius plot of the surface specific oxidation rates for this study in comparison with selected prior studies.

For the range of temperatures studied, the rate of oxidation of biodiesel soot (line a in Figure 7) was $\sim$6 times faster than that of D2 diesel soot (line b) (*29*). The activation energy for biodiesel soot was 89 kJ mol^{-1}, a little lower than that of D2,

108 kJ mol^{-1}, while the frequency factor was about 2–3 times higher for biodiesel. Our previous studies gave an oxidation rate of ethylene diffusion flame soot (line e) (*41*) that agreed with the well-established Nagle and Strickland-Constable (1962) oxidation rate of pyrographite rod (f), whereas the oxidation rate of the D2 diesel soot was lower at the temperatures studied and had a lower activation energy (*29*). To resolve some of the observed differences between the oxidation characteristics of flame vs diesel soot, Kim et al. (*43*) measured oxidation rates of flame soot with and without Fe doping. They found flame soot with Fe doping had a significantly lowered activation energy (116 kJ mol^{-1}), and in line with diesel derived soot ($\sim$110 kJ mol^{-1}), as compared with undoped flame soot (164 kJ mol^{-1}) and lowered oxidation rate. This result suggested that small amounts of metals during diesel combustion play a significant role in diesel soot abatement. The oxidation rates of metal dosed diesel soot (c and d) (*28, 35*) showed higher frequency factors than but similar activation energies to undosed D2 diesel. Other oxidation data (g, h, i, j, and k) from selected prior works are

also plotted for comparison. A major difference between our studies and other works is that we oxidized suspended particles directly, with little heat or mass transfer limitation, whereas many other works used TGA methods that may be subject to heat and mass transfer limitations associated with bulk soot samples (*28*).

It is uncertain why the oxidation kinetics of D2 diesel soot are so different from that of ethylene soot but the similar activation energies of D2 soot, metal doped D2 soot, and biodiesel soot suggest a common factor. Traces of metals from the lube oil present in both D2 and biodiesel soot, and present in larger quantities in metal dosed D2 soot, may play a role in the oxidation kinetics differences. It is reasonable to assume that lube oil consumption was essentially the same for the D2 and biodiesel tests, since both tests were done using the same engine under the same speed and load conditions. The soot mass emissions using biodiesel are roughly a factor of 5 lower than for D2. Under normal conditions, most of the lube oil ash emitted by a diesel engine becomes associated with accumulation mode soot. Thus ash content of biodiesel soot should be much higher than that of D2 diesel soot. This may explain why the oxidation rates of biodiesel soot are similar to those of lube oil dosed D2 soot (c). Retailleau et al. (*44*) found that a cerium additive catalyzed diesel soot oxidation at least partially through facilitating the formation of surface oxygen complexes on diesel soot particles. Lube oil metals might play a similar role in our study. Of course fuel oxidation, soot formation, and soot properties are expected to be different for D2 and biodiesel, making it difficult to assess the relative importance of differences in inherent soot properties and its ash content. Vander Wal and Tomasek (*45, 46*) reported that soot generated by oxygenated fuel has a nanostructure with more reactive sites for oxidation, which makes it burn much faster compared to soot made by their reference fuel. Boehman et al. (*47*) compared reactivity and nanostructure of both diesel soot and biodiesel soot. They found biodiesel soot has higher reactivity and more amorphous nanostructure, which is consistent with Vander Wal and Tomasek's finding. Further investigation, including ash analysis and high-resolution transmission electron micrography (HRTEM) analysis to quantify the differences in ash content and nanostructure, would be beneficial to the understanding of biodiesel soot's higher reactivity. Our current study was limited to one engine condition and one biodiesel fuel, SME B100. It demonstrates the utility of the HTO-TDMA method in studying biodiesel oxidation kinetics. However, more work is needed with other types of biodiesel and other engines and conditions to establish more general results.

Acknowledgments

Literature Cited

(1) Song, J.; Alam, M.; Boehman, A. Effect of alternative fuels on soot properties and regeneration of diesel particulate filters. In *Proceedings of the DEER Conference*; 2005.

(2) Song, J.; Alam, M.; Boehman, A. L.; Miller, K. Characterization of diesel and biodiesel soot. *ACS Prepr.* **2004**, *49*, 767−769.

(3) Mahadevan, R.; Lee, D.; Sakurai, H.; Zachariah, M. R. Measurement of condensed-phase reaction kinetics in the aerosol phase using single particle mass spectrometry. *J. Phys. Chem. A.* **2002**, *106*, 11083−11092.

(4) Mayer, A.; Czerwinski, J.; Wyser, M.; Mattrel, P.; Heitzer, Impact of RME/diesel blends on particle formation, particle filtration and PAH emissions. *SAE Tech. Pap. Ser.* **2005**, 2005−2001−1728.

(5) Wang, S. C.; Flagan, R. C. Scanning electrical mobility spectrometer. *Aerosol Sci. Technol.* **1990**, *13*, 230−240.

(6) Graboski, M. S.; McCormick, R. L. Combustion of fat and vegetable oil derived fuels in diesel engines. *Prog. Energy Combust. Sci.* **1998**, *24*, 125−164.

(7) Babu, A. K.; Devaradjane, G. Vegetable oils and their derivatives as fuels for CI engines: An overview. *SAE Tech. Pap. Ser.* **2003**, 2003−2001−0767.

(8) Schröder, O.; Krahl, J.; Munack, A.; Bünger, J. Environmental and health effects caused by the use of biodiesel. *SAE Tech. Pap. Ser.* **1999**, 1999−1901−3561.

(9) Monyem, A.; Van Gerpen, J. H. The effect of biodiesel oxidation on engine performance and emissions. *Biomass Bioenergy* **2001**, *20*, 317−325.

(10) Bagley, S. T.; Gratz, L. D.; Johnson, J. H.; McDonald, J. F. Effects of an oxidation catalytic converter and a biodiesel fuel on the chemical, mutagenic, and particle size characteristics of emissions from a Diesel engine. *Environ. Sci. Technol.* **1998**, *32*, 1183−1191.

(11) Krahl, J.; Munack, A.; Schröder, O.; Stein, H.; Bünger, J. Influence of biodiesel and different designed diesel fuels on the exhaust gas emissions and health effects. *SAE Tech. Pap. Ser.* **2003**, 2003−2001−3199.

(12) McDonald, J. F.; Purcell, D. L.; McClure, B. T.; Kittelson, D. B. Emissions characteristics of soy methyl ester fuels in an IDI compression ignition engine. *SAE Tech. Pap. Ser.* **1995**, 950400.

(13) Purcell, D. L.; McClure, B. T.; McDonald, J. F.; Basu, H. N. Transient testing of soy methyl ester fuels in an indirect injection, compression ignition engine. *J. Am. Oil Chem. Soc.* **1996**, *73*, 381.

(14) McCormick, R. L. Effects of biodiesel on NO$_x$ emissions; Presented at California Air Resources Board; U.S. Department of Energy, National Renewable Energy Laboratory: Golden, CO, 2005; http://www.nrel.gov/vehiclesandfuels/npbf/pdfs/38296.pdf.

(15) Bouche, T.; Hinz, M.; Pittermann, R.; Herrmann, M. Optimising tractor C1 engines for biodiesel operation. *SAE Spec. Publ.* **2000**, *SP-1545*, 57−64.

(16) McCormick, R. L.; Alvarez, J. R.; Graboski, M. S.; Tyson, K. S.; Vertin, K. Fuel additive and blending approaches to reducing NOx emissions from biodiesel. *SAE Tech. Pap. Ser.* **2002**, 2002−2001−1658.

(17) Yoshimoto, Y.; Tamaki, H. Reduction of NOx and smoke emissions in a diesel engine fueled by biodiesel emulsion combined with EGR. *SAE Spec. Publ.* **2001**, *SP-1608*, 225−233.

(18) Tat, M. E.; Van Gerpen, J. H. Biodiesel blend detection with a fuel composition sensor. *Appl. Eng. Agric.* **2003**, *19*, 125−131.

(19) Szybist, J. P.; Boehman, A. L.; Taylor, J. D.; McCormick, R. L. Evaluation of formulation strategies to eliminate the biodiesel NOx effect. *Fuel Process. Technol.* **2005**, *86*, 1109−1126.

(20) Kinney, A. J.; Clemente, T. E. Modifying soybean oil for enhanced performance in biodiesel blends. *Fuel Process. Technol.* **2005**, *86*, 1137−1147.

(21) Finch, G. L.; Hobbs, C. H.; Blair, L. F.; Barr, E. B.; Hahn, F. F.; Jaramillo, R. J.; Kubatko, J. E.; March, T. H.; White, R. K.; Krone, J. R.; Ménache, M. G.; Nikula, K. J.; Mauderly, J. L.; Van Gerpen, J.; Merceica, M. D.; Zielinska, B.; Stankowski, L.; Burling, K.; Howell, S. Effects of subchronic inhalation exposure of rats to emissions from a diesel engine burning soybean oil-derived biodiesel fuel. *Inhalation Toxicol.* **2002**, *14*, 1017−1048.

(22) Williams, J. B. Production of biodiesel in Europe − the markets. *Eur. J. Lipid Sci. Technol.* **2002**, *104*, 361−362.

(23) Korbitz, W. Biodiesel production in Europe and north America, an encouraging prospect. *Renewable Energy* **1999**, *16*, 1078−1083.

(24) Pereira, R. L.; Maria, W. H. Current status of biodiesel development in Brazil. *Appl. Biochem. Biotechnol.* **2005**, *121*, 807.

(25) Brazil to export vegetable oil-based biodiesel, says president Lula da Silva, 2004; http://www.soyatech.com/bluebook/news/viewarticle.ldml?a=20041214−20041216

(26) Monyem, A.; Van Gerpen, J. H.; Canakci, M. The effect of timing and oxidation on emissions from biodiesel-fueled engines. *Trans. ASAE* **2001**, *44*, 35−42.

(27) Jung, H.; Kittelson, D. B.; Zachariah, M. R. The influence of engine lubricating oil on diesel nanoparticle emissions and kinetics of oxidation. *SAE Tech. Pap. Ser.* **2003**, 2003−2001−3179.

(28) Higgins, K. J.; Jung, H.; Kittelson, D. B.; Roberts, J. T.; Zachariah, M. R. Kinetics of diesel nanoparticle oxidation. *Environ. Sci. Technol.* **2003**, *37*, 1949−1954.

(29) Abdul-Khalek, I.; Kittelson, D. B.; Brear, F. The influence of dilution conditions on diesel exhaust particle size distribution measurements. *SAE Tech. Pap. Ser.* **1999**, 1999−1901−1142.

(30) Khalek, I. A.; Kittelson, D. B.; Brear, F. Nanoparticle growth during dilution and cooling of diesel exhaust: Experimental investigation and theoretical assessment. *SAE Tech. Pap. Ser.* **2000**, 2000−2001−0515.

(31) Abdul-Khalek, I.; Kittelson, D. B. Real time measurement of volatile and solid exhaust particles using a catalytic stripper. *SAE Tech. Pap. Ser.* **1995**, 950236.

(32) Ng, I. P. Aethalometer performance with diesel particles. Masters thesis, University of Minnesota, Twin Cities, MN, 2002.

(33) Kittelson, D. B.; Watts, W. F.; Savstrom, J. C.; Johnson, J. P. Influence of a catalytic stripper on the response of real time aerosol instruments to diesel exhaust aerosol. *J. Aerosol. Sci.* **2005**, *36*, 1089−1107.

(34) Jung, H.; Kittelson, D. B.; Zachariah, M. R. The influence of a cerium additive on ultrafine diesel particle emissions and kinetics of oxidation. *Combust. Flame* **2005**, *142*, 276−288.

(35) Kittelson, D. B. Engines and nanoparticles: A review. *J. Aerosol Sci.* **1998**, *29*, 575−588.

(36) Hallgren, B. E.; Heywood, J. B. Effects of oxygenated fuels on DI diesel combustion and emissions. *SAE Tech. Pap. Ser.* **2001**, 2001−2001−0648.

(37) Kitamura, T.; Ito, T.; Senda, J.; Fujimoto, H. Mechanism of smokeless diesel combustion with oxygenated fuels based on the dependence of the equivalence ratio and temperature on soot particle formation. *Int. J. Engine Res.* **2002**, *3*, 223−248.

(38) Sakurai, H.; Park, K.; McMurry, P. H.; Zarling, D. D.; Kittelson, D. B.; Ziemann, P. J. Size-dependent mixing characteristics of volatile and nonvolatile components in diesel exhaust aerosols. *Environ. Sci. Technol.* **2003**, *37*, 5487−5495.

(39) Abdul-Khalek, I. S.; Kittelson, D. B.; Graskow, B. R.; Wei, Q.; Brear, F. Diesel exhaust particle size: Measurement issues and trends. *SAE Tech. Pap. Ser.* **1998**, 980525.

(40) Higgins, K. J.; Jung, H.; Kittelson, D. B.; Roberts, J. T.; Zachariah, M. R. Size-selected nanoparticle chemistry: Kinetics of soot oxidation. *J. Phys. Chem. A* **2002**, *106*, 96−103.

(41) Park, K.; Cao, F.; Kittelson, D. B.; McMurry, P. H. Relationship between particle mass and mobility for diesel exhaust particles. *Environ. Sci. Technol.* **2003**, *37*, 577−583.

(42) Kim, S. H.; Fletcher, R. A.; Zachariah, M. R. Understanding the difference in oxidative properties between flame and diesel soot nanoparticles: The role of metals. *Environ. Sci. Technol.* **2005**, *39*, 4021.

(43) Retailleau, L.; Vonarb, R.; Perrichon, V.; Jean, E.; Bianchi, D. Catalytic oxidation of a diesel soot formed in the presence of a cerium additive. I. Characterization of the cerium fraction using magnetic susceptibility and temperature-programmed desorption. *Energy Fuels* **2004**, *18*, 872−882.

(44) Vander Wal, R. L.; Tomasek, A. J. Soot oxidation: dependence upon initial nanostructure. *Combust. Flame* **2003**, *134*, 1−9.

(45) Vander Wal, R. L.; Tomasek, A. J. Soot nanostructure: Definition, quantification and implication. AAAR: Atlanta, GA, 2004.

(46) Boehman, A. L.; Song, J.; Alam, M. Impact of biodiesel blending on diesel soot and the regeneration of particulate filters. *Energy Fuels* **2005**, *19*, 1857−1864.

(47) Nagle, J.; Strickland-Constable, R. F. Oxidation of carbon between 1000 and 2000 °C. In *Fifth Carbon Conference*; Pergamon: Oxford, 1962; pp 154−164.

(48) Miyamoto, N.; Hou, Z.; Ogawa, H. Catalytic effects of metallic fuel additives on oxidation characteristics of trapped diesel soot. *SAE Tech. Pap. Ser.* **1988**, 881224.

(49) Gilot, P.; Bonnefoy, F.; Marcuccilli, F.; Prado, G. Determination of kinetic data for soot oxidation. Modeling of competition between oxygen diffusion and reaction during thermogravimetric analysis. *Combust. Flame* **1993**, *95*, 87.

(50) Neeft, J. P. A.; Nijhuis, T. X.; Smakman, E.; Makkee, M.; Moulijin, J. A. Kinetics of the oxidation of diesel soot. *Fuel* **1997**, *76*, 1129.

(51) Otto, K.; Sieg, M. H.; Zinbo, M.; Bartosiewicz, L. The oxidation of soot deposits from diesel engines. *SAE Tech. Pap. Ser.* **1980**, 800336.

(52) Ahlström, A. F.; Odenbrand, C. U. I. Combustion characteristics of soot deposits from diesel engines. *Carbon* **1989**, *3*, 475.